Ultraporous Nitrogen-Rich Carbon Nanosheets Derived from the Synergy of Eutectic Liquid and Zeolitic Imidazolate for Energy Applications

Yuan Wang[1, ‡], Xitong Chen[2, ‡], Quan-Guo Zhai[2], Jian Guo[2], Pingyun Feng[1, 2, *]

1. Materials Science and Engineering Program, University of California, Riverside, 900 University Ave, Riverside, CA 92521, United States

2. Department of Chemistry, University of California, Riverside, 900 University Ave, Riverside, CA 92521, United States

*Corresponding Author, E-mail: pingyun.feng@ucr.edu

‡These authors contributed equally to this work.

Abstract: Reported here is a unique and novel synthetic method for the preparation of highly porous nitrogen-rich carbon nanosheets from ZIF-8 (ZIF, zeolitic imidazolate framework) with the assistance of eutectic liquid. Due to the low melting temperature, a mixture of eutectic salts can provide a special atmosphere for the carbonization process and function as the template to support the ZIF-8 framework. The formation of the ultraporous nanosheets can be ascribed to the excellent miscibility between the eutectic salts and ZIF-8 framework, thus helping convert the ordered calcined intermediate species into extended carbon sheets at high temperature while inheriting the microporous structure from the prototypical ZIF-8. By controlling the ratio of eutectic liquid to ZIF-8 framework, the BET surface area of carbon nanosheets can be systematically tuned, with the highest BET surface area up to 2960 $m^2 g^{-1}$. In addition to this impressive high surface area, the pore size distribution follows well with the pristine ZIF-8. The nitrogen content varies from 9.9 wt. % to 13.4 wt. %. These characteristics contribute to the

excellent performance of CO_2 adsorption (5.45 mmol g^{-1} at 1atm and 273K) and oxygen reduction reaction (ORR) catalysis due to the large numbers of accessible active sites.

Keywords: Ultraporous carbon material, ZIF derivative, carbon dioxide capture, oxygen reduction reaction

1. Introduction

It is highly in demand to develop the ultraporous, especially microporous, carbon materials with rich numbers of heteroatoms doping for energy applications, such as electrocatalysis, carbon dioxide capture, supercapacitors and lithium ion storage.[1-5] The ultraporous structure can provide not only more accessible surface area, but also more exposed active sites to the guest molecules or reactive species.[6,7] The doped heteroatoms, such as nitrogen, can produce the basic active sites, which have strong interaction with acidic species, or break the electroneutrality of carbon materials, thus leading to the creation of charges and spin redistribution, which is favorable for electrocatalysis.[8-12]

Here we developed a novel method by the assistance of eutectic liquids for the fabrication of nitrogen doped carbon materials through the pyrolysis of ZIF-8. The as-prepared materials possessed five features: 1) ultrahigh surface area, 2) microporous carbon structure, 3) high nitrogen content, 4) uniform pore size distribution which is the same as the pristine material, 5) systematic tuning of surface area. The work reported here explored the relationship between the ratio of eutectic salts to precursors and the resulting BET surface area, nitrogen content and porous features of carbon materials.

The doped nitrogen atoms endow the materials with the ability to trap acidic gas molecules, such as CO_2. Compared with chemisorption, physisorption of CO_2 can provide the regeneration of adsorbents by applying minimal heat or through the vacuum swing adsorption process at room temperature.[13,14] Of various adsorbents, carbon based material has attracted much interest due to its low cost, lightweight, high hydrophobicity, and high physiochemical stability.[15-17] The porous structure of carbon materials can enable fast gas diffusion and provide high surface area. Here two factors can highly affect CO_2 capture ability: 1) pore size confinement effect, 2) doped nitrogen atom leading to basicity and charge delocalization in the vicinity of the carbon matrix which is favorable for the absorbing of acidic CO_2 molecules.

To eliminate CO_2 emission, the development of new energy sources with zero CO_2 emission is essential. The products of emerging technologies, such as fuel cells and metal–air batteries, have been widely considered as the most promising alternatives to conventional energy sources due to their high efficiency, no pollution, and short construction period.[18-20] ORR at cathode in fuel cells and metal-air batteries is the major barrier of these creative inventions owing to the inherently sluggish kinetics. The nitrogen doped carbon materials can also show excellent ORR activity. Currently, Pt and Pt-based alloys with high current density and activity for ORR are still the best candidates under alkaline and acidic conditions. However, due to the scarcity, the high cost, as well as the poor durability and methanol tolerance, it is not suitable for large scale commercialization. Carbon based materials have been regarded as the most promising candidate due to its high surface area, tunable porous structure, excellent

electrical conductivity, long term stability and low price compared to other materials.[21-24] Especially for the porous carbon materials, large surface area and porous structural feature can introduce more accessible active sites and facilitate the transportation of electrons and oxygen species.[25] Particularly, nitrogen doped carbon materials which can break the electroneutrality of the carbon matrix, can create charge redistribution favorable for oxygen adsorption and reduction.[26-30]

Traditional methods for preparation of porous heteroatom doped carbon materials include direct pyrolysis of the mixed carbon and doping atom precursors. In addition, porous materials such as mesoporous silica materials, Ni foam or melamine foam have been widely applied as templates and/or precursors for the introduction of high surface area, hierarchical porous structure, and rich numbers of exposed active sites in the carbon materials. However, it is hard to control the pore size or get high surface area materials when adopting these templates. Metal-organic frameworks (MOFs), as a new class of crystalline porous materials with high surface area, well-defined structure and uniform pore distribution, are unique candidates functioning both as precursors and templates for fabricating highly porous heteroatom doped carbon materials.[31-35] However, the calcined products of MOFs tend to lose some of the unique features due to the agglomeration and aggregation of the carbon materials. Moreover, the frameworks will be much possibly collapsed before the carbonization temperature, thus failing to keep the porous structure with the prototypical pore size, especially the microporous property.

To maintain the high surface area and porous structure of MOFs through the high temperature pyrolysis, here, a facile and simple MOFs calcination in molten salt for the fabrication of ultraporous nitrogen-rich carbon materials with hierarchical porosity is presented. A mixture of eutectic salts NaCl-$ZnCl_2$ (with a NaCl molar ratio of 33%, **Figure S1**) is employed as template to help sustain the structure feature of ZIF-8. Since the low melting temperature of eutectic salts, it can diffuse into the sodalite cage of ZIF-8 at a relatively low temperature and remain liquid form during calcination in inert atmosphere. It is envisaged that the liquid salts may have a better miscibility with MOFs and could provide an environment for the orderly distribution with the following extension of calcined intermediate species, resulting in the formation of extended carbon sheets while keeping the high surface area and microporous feature of the ZIF-8. After the high temperature carbonization process, the mixture of salts in the pores can be easily removed, leading to nitrogen doped porous carbon materials. Based on the different ratios of eutectic salts to ZIF-8 during the high temperature pyrolysis, a systematic tuning of BET surface area but with relatively similar nitrogen content and pore size distribution of nitrogen doped carbon materials can be obtained. It is worth mentioning that the highest surface obtained here is 2965 $m^2 g^{-1}$, which is among the highest values in carbon materials. Moreover, the structures of micropores of ZIF-8 can be retained after the calcination process. The obtained carbon based materials with tunable properties are studied for CO_2 adsorption and ORR performance.

2. Experimental Section

2.1 Synthesis of ZIF-8 Nanocrystals

The synthesis of ZIF-8 nanocrystals is based on a previous procedure. Typically, $Zn(NO_3)_2 \cdot 6H_2O$ (1.68 g) is dissolved in 80 mL of methanol. A mixture of 2-methylimidazole (3.70 g) with 80 mL methanol is added to the above solution with vigorous stirring for 24 h. The product is separated by centrifugation and washed thoroughly with methanol for twice, and finally dried overnight at 50 °C in vacuum. (Yield: 0.69g; 54% based on Zn)

2.2 Synthesis of carbon materials

In a typical approach 500 mg of ZIF-8 is used as precursor. The mixtures with varied ratios between sodium chloride, zinc chloride and ZIF-8 are freshly prepared by grinding prior to the experiment. The precursor is thoroughly mixed with the salt mixture, transferred to a ceramic crucible, and heat-treated under argon atmosphere in a chamber furnace. All the samples are heated to 900 °C and kept for 3 h at this temperature. After cooling to room temperature, the material is grinded, etched in 10 wt. % HCl overnight, and dried in vacuum at 60 °C for 12 hours. (The yield of all samples is around 50mg, 10%)

2.3 Electrocatalytic activity measurements

Electrochemical characterization of the catalysts is performed in a conventional three-electrode cell using CHI760D electrochemical workstation (CH Instruments, USA) controlled at room temperature and under atmospheric pressure. Ag/AgCl and platinum wire are used as reference and counter electrodes, respectively. All potentials in this report are converted into reversible hydrogen electrode (RHE).

A ring-disk electrode (RDE) with a glassy carbon disk and a Pt ring is served as the substrate for the working electrode. The catalyst ink is prepared by mixing the catalyst powder (10 mg) with 80 μL Nafion solution (5wt %) and 1.2 ml ethanol in an ultrasonic bath. Then 20 μL of catalyst ink is pipetted onto the GC electrode in 0.1 M KOH corresponding a catalyst loading of 0.6 mg cm^{-2}. In 0.1M $HClO_4$ solutions, 20 μL of catalyst ink is deposited onto the GC electrode corresponding a catalyst loading of 0.6 mg cm^{-2}. As a comparison, commercial 20 wt. % platinum on Vulcan carbon black (Pt/C from Alfa Aesar) is prepared by blending Pt/C (10 mg) with 80 μL Nafion solution (5wt %) and 1.2 ml ethanol in an ultrasonic bath. A Pt loading about 20 μg cm^{-2} is applied in both alkali and acid conditions.

Linear sweep voltammetry (LSV) polarization curves for the oxygen reduction reaction (ORR) are measured in an oxygen saturated 0.1 M KOH and 0.1 M $HClO_4$ electrolyte with a sweep rate of 10 mV s^{-1} at various rotating speeds from 400 to 2500 rpm. The cyclic voltammogram (CV) are recorded in solutions saturated with either Ar or O_2 gas without rotation with same sweep rate as that of LSV curve. The electron transfer number (n) and kinetic current density (j_K) are analyzed on the basis of Koutecky– Levich equations shown in below:

$$1/j=1/j_L+1/j_K$$

$$j_L=0.62nFCD^{2/3}\upsilon^{-1/6}w^{-1/2}=Bw^{-1/2}$$

$$1/j=1/Bw^{-1/2}+1/j_K$$

where $B=0.62nFC_0 D_0^{2/3} \upsilon^{-1/6}$, j is the measured current density, j_K and j_L are the kinetic- and diffusion-limiting current densities, *w* is the rotation speed, *n* is the electron transfer number, *F* is the Faraday constant (F = 96485 C mol^{-1}), C is the bulk concentration of O_2, D is the diffusion coefficient of dissolved oxygen, v is the kinematic viscosity of the electrolyte.

2.4 Characterization

The crystal structures of the materials are characterized by X-ray diffractometer (XRD) (D/Max2000, Rigaku) using a Bruker D8-Advance powder diffractometer operating at 40 kV, 40 mA for Cu Kα radiation (λ=1.5406 Å). The morphology and composition of the samples are analyzed with a Tecnai T12 transmission electron microscope (TEM). CO_2, N_2 and H_2 adsorption results under a certain temperature and pressure are obtained using an ASAP 2020 analyzer (Micromeritics, USA). The specific surface areas are calculated using the Brunauer–Emmett–Teller (BET) equation from the nitrogen adsorption data in the relative range (P/P_0) of 0.04-0.20. The pore size distribution (PSD) plot is recorded from the adsorption and desorption branch of the isotherm based on the Barrett–Joyner–Halenda (BJH) and Horvath-Kawazoe (H-K) model. The elemental analysis is performed in UCR.

3. Results and Discussion

3.1 Structural Characteristics and Chemical Properties of Porous Carbons

A schematic diagram describing the structure of ZIF-8 is shown in **Figure S2**. ZIF-8 has a sodalite-type structure with a cavity dimension of 11.6 Å and small pore apertures of 3.4 Å. ZIF-8 is chosen as the typical precursor among MOF materials due to its high

surface area, high chemical and thermal stability. Moreover, the nitrogen source in the ligand can lead to in-situ synthesis of nitrogen doped carbon materials. Eutectic salt NaCl-$ZnCl_2$ (with a NaCl mole ratio of 33%) are selected as template to mix with ZIF-8 since it is cheap, abundant, harmless, and inert toward carbon at high temperatures and more importantly with low melting temperature it can be easily removed. Varied ratios of ZIF-8 to eutectic salts are prepared from 1:0, 1:1, 1:2, 1:3, 1:4, 1:5, 1:10 and 1:15. After grinding ZIF-8 and eutectic salts together, the mixtures are calcined at 900 °C in Ar atmosphere for 3 hours. Then the obtained materials are etched with 10 wt. % HCl overnight. The different carbon materials obtained here are collectively labeled as NC (x: y), where NC stands for nitrogen doped carbon, and x: y stands for the mass ratio of ZIF-8 to NaCl-$ZnCl_2$ salts.

The influence of different mass ratios of ZIF-8 to NaCl-$ZnCl_2$ salts is firstly studied. The powder X-ray diffraction (PXRD) patterns show that after high temperature pyrolysis and etching process, ZIF-8 are transformed to carbon materials possessing graphitic carbon structure feature with the (002) and (100) planes appearing at 26.1° and 43.2° (**Figure S3**).[22,36] As the ratio of ZIF-8 to NaCl-$ZnCl_2$ salts decreases, the crystallinity remains similar with only a minor decrease. Such high degree of graphitization is beneficial to the electrical conductivity of the carbon material, which could be helpful for the improvement of ORR activity. No diffraction peaks of impurities could be observed, suggesting the complete conversion of carbon materials and removal of template salts after the heat treatment of ZIF-8 and etching in acidic solution.

Microscopic morphology and porous structure of ZIF-8 and corresponding NC (x: y) are imaged by transmission electron microscopy (TEM) (Figure 1). As revealed in **Figure 1a**, ZIF-8 with the geometric shape of rhombic dodecahedra and an average size of 50 nm to 70 nm is prepared, similar to those in the previous report.[6] Through the direct pyrolysis of composites with a ratio of ZIF-8 to eutectic salts about 1: 10 at 900 °C in Ar atmosphere and after acid etching, NC (1:10) consisting of extended carbon sheets with a micropore dominated structure can be obtained (**Figure 1b**). Further inspection using high-resolution transmission electron microscopy (HRTEM) confirms that the obvious distinct nanovoids are distributed over the entire area of carbon sheets, verifying the microporous structure of the carbon materials (**Figure 1c**). The porous features with large surface areas are favorable for excellent electrolyte and oxygen diffusion in ORR activity. In addition, it indicates that NC (1:10) carbon sheets feature a carbon graphitic crystalline structure, as seen by the distinct lattice fringes with a spacing of 0.34 nm, corresponding with the (002) plane of graphite (**Figure 1c**). The morphologies of other NC (x: y) are also studied (**Figure S4**). It is interesting that NC (1:0) (ZIF-8 pyrolyzed without the eutectic salts) consist of disordered aggregated nanoparticles (**Figure 1d**). However, after the addition of eutectic salts, the NC (x: y) shows extended carbon sheets. The distinct nanovoids are also seen in the other NC (x: y) materials, indicating the contribution of the eutectic salts to the porous structure of the obtained carbon materials (**Figure S5**). It is also worth mentioning that the carbon materials obtained with eutectic salts and without eutectic salts have dramatically different morphologies.

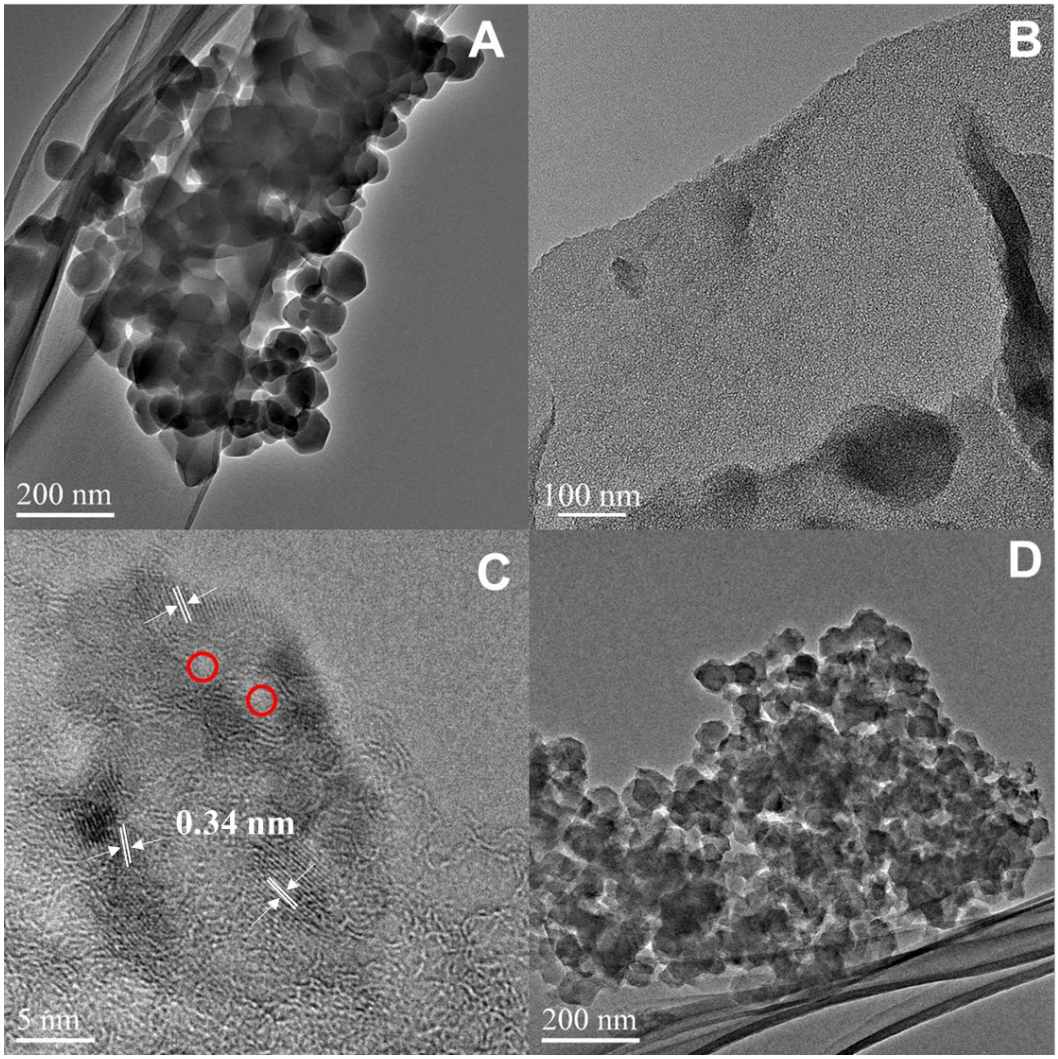

Figure 1. a) TEM image of ZIF-8 nanoparticles. b, c) TEM and HRTEM images of derived carbon materials NC (1:10). d) TEM image of NC (1:0).

2-methylimidazole (2-MIM) ligands in the ZIF-8 provide rich nitrogen source and are responsible for the formation of C–N/C=N moieties on the surface of the NC (x: y) which are superior for the ORR activity.[37] Regarding the chemical composition of the NC (x: y), all samples show high nitrogen contents between 9.9 wt. % to 13.4 wt. % by elemental analysis (**Table 1**). Such high nitrogen contents are higher than most of the reported nitrogen doped carbon materials.[38-40] X-ray photoelectron spectroscopy (XPS) was also

conducted to gain deeper insights on the chemical state of the nitrogen. According to the survey spectra of NC (1:10), it consists of carbon, nitrogen and oxygen. The N1s peaks are deconvoluted into three different types of nitrogen species: pyridinic-N (N1, 398.3 ± 0.1 eV), pyrrolic-N (N2, 400.0 ± 0.1 eV), and graphitic-N (N3, 401.0 ± 0.1 eV) (**Figure 2a,b**).[39] The similar deconvolution of N1s peaks of other NC (x: y) are also conducted and information related to the type and content of the nitrogen species present in the NC (x: y) is shown in **Figure 2a, b** and summarized in **Table 1** as well. The pyridinic-N and graphitic-N are reported to play a crucial role in oxygen reduction. The high content of pyridinic-N and graphitic-N of NC (1:10) will lead to high catalytic activity. It was found that when changing the ratios of ZIF-8 to eutectic salts, the total nitrogen contents do not alter so much. All NC (x: y) samples contain qualitatively and quantitatively similar N sites. This is reasonable in considering that the eutectic salts added are not participating in any reactions and are removed completely from the final products. A Raman spectroscopy of NC (1:10) is also give in **Figure S7**. Two obvious peaks were found at 1340 and 1590 cm^{-1}, which were assigned to the D-band (defective sp^3 carbon) and G-band (graphitic sp^2 carbon). The intensity ratio I_D/I_G can show the defect level of carbon atoms in the materials. The considerable amount of defects in NC (1:10) is demonstrated by the relatively high ratio of I_D/I_G in the Raman spectrum, which is 0.96.

Table 1. Elemental compositions of the porous NC (x: y) materials by elemental analysis and XPS analysis.

NC (x: y)	Elemental analysis		XPS analysis		
	N (wt. %)	C (wt. %)	Pyridinic-N (at. %)	Pyrrolic-N (at. %)	Graphitic-N (at. %)
1: 0	13.4	71.3	0.35	0.35	0.30
1: 1	11.9	77.4	0.29	0.22	0.49
1: 2	11.6	78.4	0.38	0.21	0.41

1: 3	10.9	79.4	0.37	0.17	0.46
1: 4	11.3	79.3	0.29	0.28	0.43
1: 5	11.8	79.0	0.28	0.19	0.53
1: 10	11.8	76.5	0.35	0.24	0.41
1: 15	9.9	77.9	0.22	0.10	0.68

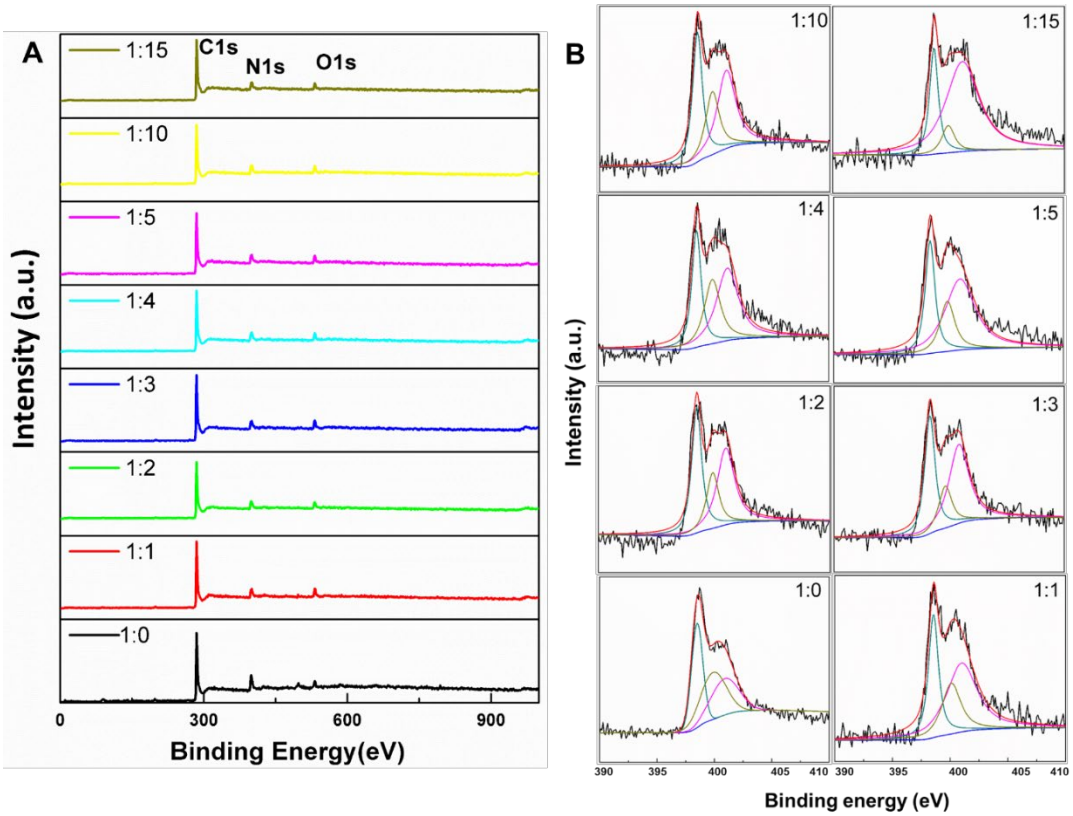

Figure 2. a) Survey scanned XPS spectrum and b) deconvoluted N1s spectrum of NC (x: y). The inset in (b) shows the three kinds of chemical bonding configurations of nitrogen dopant (pyridinic-N, N1, green lines; pyrrolic-N, N2, yellow lines; and graphitic-N, N3, pink lines).

The porous properties can be further confirmed by Brunauer-Emmett-Teller (BET) measurement (**Figure 3**). The nitrogen sorption isotherm at 77K of NC (1:10) showed a typical type-I behavior, with a steep increase at low pressure, suggesting the intrinsic

microporous characteristic (**Figure 3a**). The BET surface area for NC (1:10) is 2960 m^2 g^{-1}. Note that this surface area is almost reaching the theoretical surface area of graphene which is 2965 m^2 g^{-1}.[25] The material can be regarded as three-dimensional nanographene sheets with high surface area and nitrogen doping. In addition, the BET surface area of the samples obtained at different ratios of ZIF-8 to salts shows a continuous increase as the ratio decreases (**Table 2**). Even the lowest investigated eutectic salts content in NC (1:1) still results in a surface area of 1086 m^2 g^{-1}. In comparison, the BET surface area of NC (1:0) without the help of eutectic salts shows a relatively low surface area of 896 m^2 g^{-1}.

Table 2. BET surface area, micropore surface area, micropore volume and gas uptakes of porous NC (x: y) materials.

NC (x: y)	BET surface area (m^2 g^{-1})	Micropore surface area (m^2 g^{-1})	Micropore volume (m^2 g^{-1})	CO_2 uptake at 273K (mmol g^{-1})	CO_2 uptake at 298K (mmol g^{-1})	Qst value for CO_2 (KJ mol^{-1})	H_2 uptake at 77K (wt. %)
1 : 0	897	760	0.42	5.00	3.44	32.8	1.51
1 : 1	1086	1080	0.62	5.85	3.57	32.3	1.77
1 : 2	1368	1360	0.75	5.89	3.62	31.3	2.13
1 : 3	2141	2107	1.12	5.85	3.48	29.1	2.31
1 : 4	2215	2184	1.16	5.13	3.21	31.7	2.33
1 : 5	2261	2224	1.17	5.71	2.90	32.3	2.44
1 : 10	2960	2783	1.55	5.45	3.08	31.5	2.48
1 : 15	2397	2332	1.24	5.63	3.13	34.7	2.47

Interestingly, BET analysis shows that the corresponding pore size distributions for NC (x: y) fall into 0.3 nm and 1.2 nm (**Figure 3b**). Such pore sizes are closed to those of the window size of 3.4 Å and cavity size of 11.6 Å in ZIF-8. For the NC (1:0), the nitrogen

sorption isotherm at 77K also shows a steep uptake at low relative pressure (P/P_0 <0.015), but there is a hysteresis loop at high relative pressure (P/P_0 >0.50) (**Figure 3a**). This suggests the intrinsic microporous structure of the NC (1:0) together with mesopores possibly resulting from the interparticle voids when agglomerating together. For other NC (x: y), the isotherms showed a typical type-I behavior, with the intrinsic microporous characteristic (**Figure 3a**). The large surface area and pore volume would be beneficial to the exposure of active sites and rapid transportation of ORR-relevant species (**Table 2**). In addition, this strategy presents a facile and simple way to systematically control the surface area of carbon materials based on the different ratio of salts added with MOF materials.

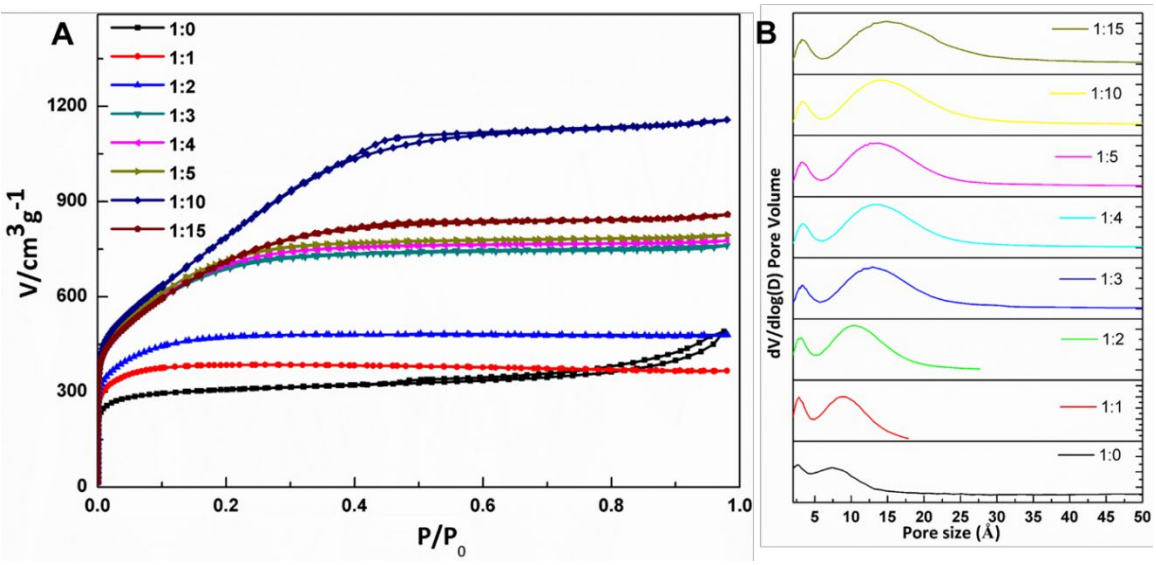

Figure 3. a) Nitrogen physisorption isotherms and b) micropore size distribution of the carbon catalysts prepared with different weight ratio between ZIF-8 and NaCl-$ZnCl_2$ salts NC (x: y).

A possible mechanism is proposed here to demonstrate the key functions of eutectic liquids. With low melting point and fluidic nature under the pyrolysis conditions, the eutectic liquids play two key roles: 1) acting as fluidic template filling in the pore space of ZIF-8 and sustaining the microporous feature during the calcination and graphitization process; 2) arranging ZIF-8 nanocrystals orderly due to the good miscibility between eutectic liquids and ZIF-8 nanocrystals. During the decomposition process, the eutectic liquids not only serve as the support to help keep the microporous structure but arrange the decomposed intermediate of the nanocrystals in an orderly arrangement, leading to the even graphitization between nanocrystals and resulting in a continuous phase with extended carbon sheets making up of stacked graphite-like layers. As can be seen above, with no addition of salts, the ZIF-8 was carbonized as aggregated carbon particles with relatively low surface area.

TEM shows that carbon materials obtained after addition of salts could be a result of a continuous phase of ZIF-8 and eutectic salts with extended carbon sheets made up of several stacked graphite-like layers, as shown in **Figure 1b** and **1c**. While with no addition of salts, the carbonization of ZIF-8 occurs as dispersed phase resulting as individual and aggregated carbon particles.

3.2 Electrocatalytic Properties

The ORR electrocatalytic activity of the NC (x: y) materials is evaluated firstly by cyclic voltammetry (CV) and rotating disk electrode (RDE) linear sweep voltammetry (LSV) measurements in both 0.1 M KOH solution and 0.1 M $HClO_4$ solution. To reflect the real current response from ORR, the CV and RDE LSV curves are corrected by subtracting

the curves recorded under saturated Ar from those in saturated O_2. To explore the ORR performance of NC (x: y) materials, RDE LSV are performed at 1600 rpm as shown in **Figure 4a**. The onsite potential of carbon materials increases as the ratio of ZIF-8 to eutectic salts decreases. Among the samples studied, the highest onset potential and largest cathodic current density are harvested by NC (1:10). The results show that the NC (1:10) material show a relatively larger onsite potential and half-wave potential than that of 20 wt. % Pt/C, suggesting its superior activity. As shown in **Figure 4b**, no obvious redox peak is observed for NC (1:10) in Ar-saturated solution from the CV curve. However, when the solution is saturated with O_2, a well-defined cathodic peak clearly appears at around 0.84 V, confirming the electrocatalytic activity for ORR. The electrochemical catalytic activities of NC (x: y) for ORR in acidic media (0.1 M $HClO_4$) are also studied. The onsite potential of carbon materials also increases as the ratio between ZIF-8 and eutectic salts decreases **Figure 4d**. In addition, NC (1:10) still has the highest onset potential and largest cathodic current density. The polarization curve of NC (1:10) in 0.1 M $HClO_4$ is displayed with the onset potential and the half-wave potential only 60 mV more negative than those of Pt/C. In the acidic cyclic voltammograms (CVs) curves, the reduction peak potential of NC (1:10) is 0.67 V, only 138 mV smaller than that of Pt/C but with a higher peak current of 3.96 mA cm^{-2}, highlighting the pronounced electrocatalytic activity of carbon nanosheets for oxygen reduction in acidic conditions (**Figure 4e**).

The selectivity of oxygen for the synthesized carbon materials is depicted in linear Koutecky–Levich (K-L) plots obtained from the polarization curves at various rotating speeds (**Figure S8a, b**). RDE experiments are performed at various rotation rates in both

O_2-saturated alkaline and acidic conditions. The electron transfer number (n) as a function of potential can be calculated from the K-L plots. The linearity of K–L plots for NC (1:10) indicates first-order reaction kinetics regarding on the concentration of dissolved oxygen and similar electron transfer numbers (n) at various potentials (**Figure S8c, d**). The value of n shows a four-electron transfer pathway for ORR catalysis, corresponding to the complete reduction of oxygen into hydroxide anions or water.[42,43]

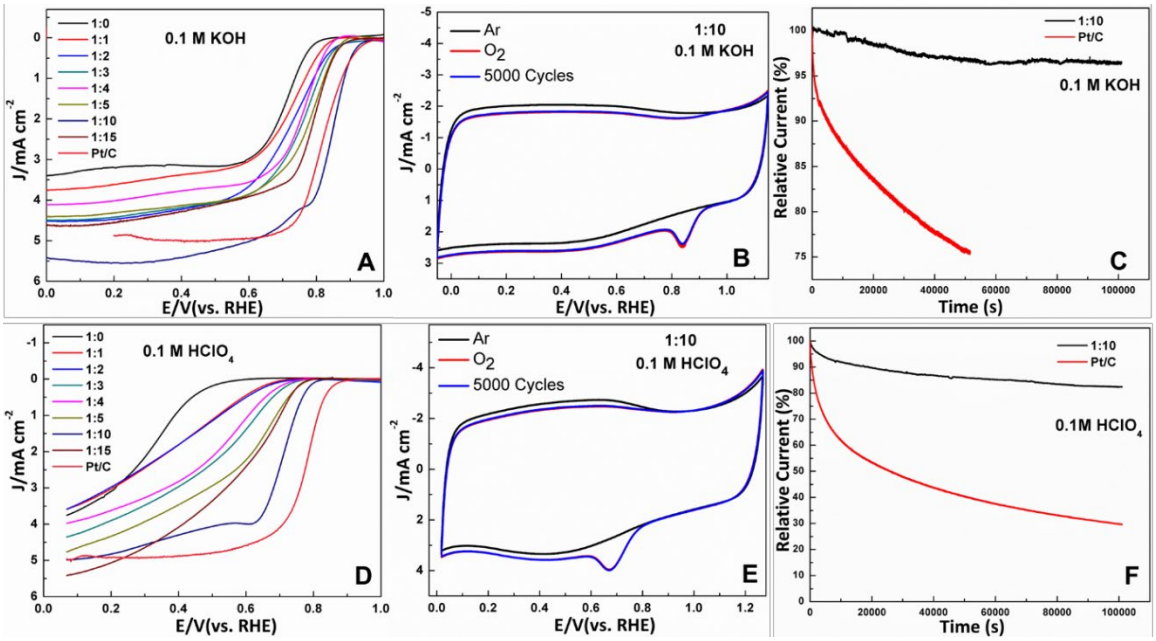

Figure 4. RDE voltammograms of NC (x: y) in O_2-saturated 0.1 M KOH (a) and in O2-saturated 0.1 M $HClO_4$ (d). Cyclic voltammograms of NC (x: y) in O_2-saturated 0.1 M KOH (b) and 0.1 M $HClO_4$ (e). The chronoamperometric responses (i–t) of NC (1:10) and Pt/C at 0.55 V vs. RHE in O_2-saturated 0.1 M KOH (c) and at 0.55 V vs. RHE in 0.1 M $HClO_4$ (f).

To evaluate the durability of NC (1:10) and compare it with Pt/C, chronoamperometric responses are measured. The stability test is conducted for NC (1:10) material by

chronoamperometry at a constant voltage of ~0.55V (vs. RHE) in O_2-saturated in alkaline and acidic condition with a rotation rate of 1600 rpm. As shown in **Figure 4c, f**, the NC (1:10) exhibits a very slow attenuation and high relative currents are remained after 100,000 s in both solutions. However, the ORR current on Pt/C declines sharply both in alkaline and acidic solutions as measured at the same conditions. Notably, NC (1:10) also shows better tolerance toward methanol than that of Pt/C in both alkaline and acidic conditions. Subsequently, the chronoamperometric responses of NC (1:10), and Pt/C are measured with the introduction of methanol to evaluate the methanol tolerance of the as-prepared porous carbons. As shown in **Figure S8e, f**, a strong response is observed for the Pt/C when methanol was added. However, the responses for NC (1:10) under the same treatment are almost negligible. Moreover, no noticeable changes are observed in the peak current or capacitive current for NC (1:10) in the corresponding cyclic voltammograms for 5000 cycles in 0.1 M KOH and 0.1 $HClO_4$ solutions (**Figure 4b, e**).

As shown above, the resultant NC (1:10) exhibits excellent ORR activity, good tolerance to methanol, and superior stability in comparison to commercial Pt/C catalyst, which might be attributed to the highly porous structures, high surface area, and favorable N composition and content with wide distribution. Compared with other reported benchmark non-precious metal catalysts, the values of onset and half wave potentials of NC (1:10) in both alkaline and acid conditions are still among the best reported to date.[8,14,20,21] Moreover, it is interesting to note that the ORR activity of the material increases as the ratio of ZIF-8 to eutectic salts decreases. As is known that two crucial factors govern the performance of carbon-based ORR catalysts. One is the intrinsic

nature of the active sites that are determined by the elemental composition and the interactions between different components. Another crucial factor is the large surface area and porous structural feature that can introduce more active sites and facilitate the transportation of electrons and oxygen species. The intrinsic nature of the active sites in obtained materials mainly relies on the nitrogen doping into the carbon matrix, creating positive charge in the adjacent carbon atoms which are favorable for oxygen adsorption and reduction. The remarkable different ORR activity of materials derived with varied salts ratio is highly interesting if we consider that they show similar nitrogen contents. The pyridinic N and graphitic N are reported to play a crucial role in oxygen reduction reaction. The high content of pyridinic N and of graphitic N in those materials, especially in NC (1:10) and NC (1:15), will lead to high catalytic activity. Another factor of different ORR performance may result from the increment of the surface area. Notably, the NC (1:10) material shows a relatively high surface area about 2960 m^2 g^{-1}. Since the nitrogen content of the materials are relatively similar between the different materials, the increasing of surface area plays an important role for the increasing ORR activity. The larger surface area can help to distribute more active sites exposed to the reactive species. In addition, the high surface area will help the mass transfer of active species. This method also presents a facile and simple way to systematically control the surface area of carbon materials for the ORR application.

3.3 Gas Adsorption Performance

Due to the high level of nitrogen doping in the synthesized carbon materials and the microporous characteristic, the materials are evaluated for their CO_2 adsorption ability.

CO_2 adsorption isotherms are collected at 1 bar at 273 and 298 K, respectively (**Figure 5a and 5b**). The results clearly demonstrate the outstanding CO_2 uptake capacity of the nitrogen doped porous carbon materials. At 273 K and 1 bar, NC (1:10) material achieves a remarkable value of 5.45 mmol g^{-1}. It also shows a high uptake about 3.08 mmol g^{-1} at 298 K. As the ratio of ZIF-8 to salts decrease, the CO_2 uptake value for the NC (x: y) does not vary too much. The data of our work is well above those reported carbon materials.[14,39,40,44] It is usually regarded that the high CO_2 uptake are correlated with two controlling parameters in the nitrogen doped carbon materials, the nitrogen content, and the ultra-fine porous structure.[23,45] Both the experiment and simulation results demonstrate that doping of nitrogen into carbon materials could create surface basic sites and enhance adsorption of acidic CO_2 molecules.[38,40] In addition, the increased surface area could provide a great area for the physi-sorption of CO_2 molecules. The nitrogen contents of different NC (x: y) are similar with each other. As discussed above, the surface area increases with the ratio of ZIF-8 to salts decreases. However, the results show that CO_2 adsorption capabilities are similar among different NC materials. As is well known, the increased surface area, especially microporous surface area could contribute favorably to the overall enhancement of the CO_2 capture performance. However, CO_2 adsorption in our NC (x: y) materials suggests a different story. This suggest the importance of nitrogen doping in carbon materials for CO_2 adsorption. The CO_2 adsorption is not always linearly proportional to the BET surface area. To have a better understanding about the strength of the interaction between CO_2 molecules and the carbon materials, the CO_2 adsorption energy (the isosteric heat of adsorption Qst) is calculated by fitting the CO_2 adsorption isotherms at 273 and 298 K for each sample to

the Clausius–Clapeyron equation.[40,46] The plots of Qst as a function of CO_2 uptake for NC (x: y) are presented in **Figure 5c**. The Qst for the different NC materials lies in the range of 29.9 - 34.8 kJ mol^{-1}, which is higher than mostly reported values for typical carbon adsorbents.[46-47] The high initial Qst values demonstrate strong interaction between CO_2 molecules and the pore walls of N-doped carbons. It is noteworthy that the Qst value is similar between different NC (x: y) materials with similar nitrogen content, implying that nitrogen functional groups play an important role in the initial interaction between CO_2 and the carbon materials.

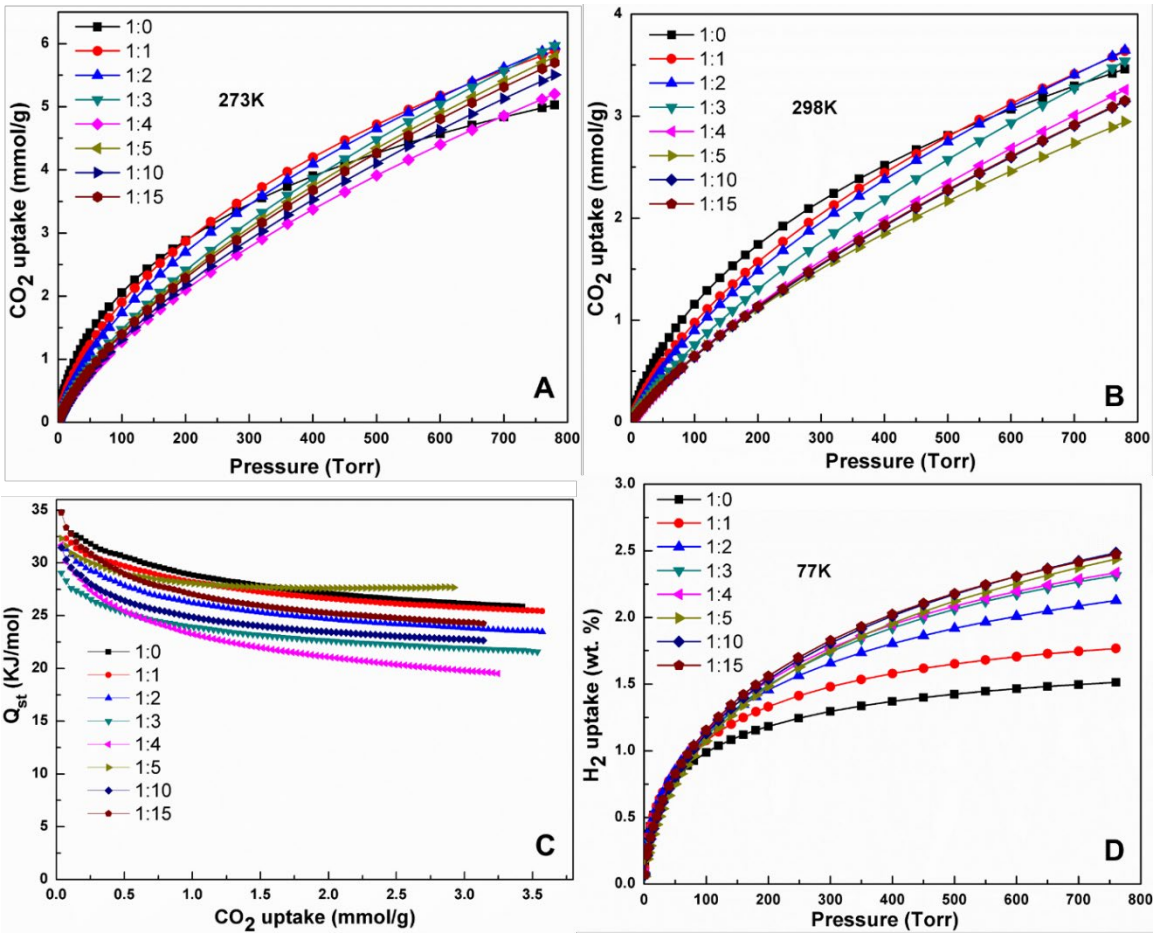

Figure 5. a) CO_2 adsorption isotherms at 273 K, b) CO_2 adsorption isotherms at 298 K, c) isosteric heat of adsorption, d) H_2 adsorption isotherms at 77 K of the NC (x: y) materials.

H_2 adsorption isotherms are also studied at 77K at 1 bar. It shows that the H_2 adsorption capacity of the different NCs is correlated to the specific surface area with a roughly linear relationship to BET surface areas. The NC (1:10) material has a maximum adsorption of 2.5 wt. %. This number is comparable to other porous carbons.[38,47-49] Different from CO_2 uptake, H_2 adsorption shows a linear relationship with surface area. Similar results in the H_2 adsorption capacity and the specific surface area of carbon materials have been verified by other reports.

4. Conclusion

In conclusion, we have demonstrated a facile and relatively green method for the preparation of ultraporous nitrogen doped carbon materials via a eutectic salt-templating process. The surface area of carbon materials could be varied systematically by simply controlling the ratio of ZIF-8 to the eutectic mixture salts. As the ratio of ZIF-8 to the eutectic mixture salts decreases, the nitrogen doped porous carbon materials have increased surface area while maintain similar nitrogen content. The material NC (1:10) has the highest surface area of 2960 $m^2 g^{-1}$ and a nitrogen content of 11.8 wt. %. It also possesses the highest H_2 adsorption of 2.5 wt. % at 77K and 1 bar and demonstrates a high ORR property, even superior to Pt/C from the viewpoint of half wave potential in alkaline solutions. In addition, this work also shows a relationship among gas sorption,

BET surface are and nitrogen content. CO_2 adsorption is not linearly dependent on the BET surface areas in nitrogen doped carbon materials. This work here paves a novel way for the fabrication of ultraporous heteroatom doped carbon materials.

Acknowledgements

The research was supported by the US Department of Energy, Office of Basic Energy Sciences, Materials Sciences and Engineering Division under Award No. DE-SC0010596 (P.F)

Reference

[1] Y.-Z. Chen, G. Cai, Y. Wang, Q. Xu, S.-H. Yu, H.-L. Jiang, Palladium nanoparticles stabilized with N-doped porous carbons derived from metal-organic frameworks for selective catalysis in biofuel upgrade: the role of catalyst wettability, Green Chem., 18 (2016) 1212-1217.

[2] B. Wu Hao, S. Wei, L. Zhang, R. Xu, H. Hng Huey, W. Lou Xiong, Embedding sulfur in MOF-derived microporous carbon polyhedrons for lithium-sulfur batteries, Chem. Eur. J., 19 (2013) 10804-10808.

[3] Z. Li, L. Yuan, Z. Yi, Y. Sun, Y. Liu, Y. Jiang, Y. Shen, Y. Xin, Z. Zhang, Y. Huang, Insight into the electrode mechanism in lithium-sulfur batteries with ordered microporous carbon confined sulfur as the cathode, Adv. Energy Mater., 4 (2014) 1301473.

[4] Y. Nie, L. Li, Z. Wei, Recent advancements in Pt and Pt-free catalysts for oxygen reduction reaction, Chem. Soc. Rev., 44 (2015) 2168-2201.

[5] D.W. Wang, F. Li, M. Liu, G.Q. Lu, H.M. Cheng, 3D aperiodic hierarchical porous graphitic carbon material for high-rate electrochemical capacitive energy storage, Angew. Chem. Int. Ed., 47 (2007) 373-376.

[6] Y.Z. Chen, C. Wang, Z.Y. Wu, Y. Xiong, Q. Xu, S.H. Yu, H.L. Jiang, From bimetallic metal-organic framework to porous carbon: high surface area and multicomponent active dopants for excellent electrocatalysis, Adv. Mater., 27 (2015) 5010-5016.

[7] A. Aijaz, J.-K. Sun, P. Pachfule, T. Uchida, Q. Xu, From a metal-organic framework to hierarchical high surface-area hollow octahedral carbon cages, Chem. Commun., 51 (2015) 13945-13948.

[8] H.-W. Liang, W. Wei, Z.-S. Wu, X. Feng, K. Müllen, Mesoporous metal-nitrogen-doped carbon electrocatalysts for highly efficient oxygen reduction reaction, J. Am. Chem. Soc., 135 (2013) 16002-16005.

[9] R. Silva, D. Voiry, M. Chhowalla, T. Asefa, Efficient metal-free electrocatalysts for oxygen reduction: polyaniline-derived N- and O-doped mesoporous carbons, J. Am. Chem. Soc., 135 (2013) 7823-7826.

[10] S. Wang , E. Iyyamperumal , A. Roy, Y. Xue, D. Yu, L. Dai, Vertically aligned BCN nanotubes as efficient metal-free electrocatalysts for the oxygen reduction reaction: A synergetic effect by co-doping with boron and nitrogen, Angew. Chem. Int. Ed., 50 (2011) 11756-11760.

[11] Y. Wang, A. Kong, X. Chen, Q. Lin, P. Feng, Efficient oxygen electroreduction: hierarchical porous Fe-N-doped hollow carbon nanoshells, ACS Catal., 5 (2015) 3887-3893.

[12] K. Sasan, A. Kong, Y. Wang, M. Chengyu, Q. Zhai, P. Feng, From hemoglobin to porous N-S-Fe-doped carbon for efficient oxygen electroreduction, J. Phys. Chem. C, 119 (2015) 13545-13550.

[13] B. Ashourirad, P. Arab, T. Islamoglu, K.A. Cychosz, M. Thommes, H.M. El-Kaderi, A cost-effective synthesis of heteroatom-doped porous carbons as efficient CO_2 sorbents, J. Mater. Chem. A, 4 (2016) 14693-14702.

[14] W. Tian, H. Zhang, H. Sun, A. Suvorova, M. Saunders, M. Tade, S. Wang, Heteroatom (N or N-S)-doping induced layered and honeycomb microstructures of porous carbons for CO_2 capture and energy applications, Adv. Funct. Mater., 26 (2016) 8651-8661.

[15] K. Li, S. Tian, J. Jiang, J. Wang, X. Chen, F. Yan, Pine cone shell-based activated carbon used for CO_2 adsorption, J. Mater. Chem. A, 4 (2016) 5223-5234.

[16] J.P. Paraknowitsch, A. Thomas, Doping carbons beyond nitrogen: an overview of advanced heteroatom doped carbons with boron, sulphur and phosphorus for energy applications, Energy Environ. Sci., 6 (2013) 2839-2855.

[17] J. Gong, H. Lin, M. Antonietti, J. Yuan, Nitrogen-doped porous carbon nanosheets derived from poly(ionic liquid)s: hierarchical pore structures for efficient CO_2 capture and dye removal, J. Mater. Chem. A, 4 (2016) 7313-7321.

[18] Q. Lai, Y. Zhao, Y. Liang, J. He, J. Chen, In situ confinement pyrolysis transformation of ZIF-8 to nitrogen-enriched meso-microporous carbon frameworks for oxygen reduction, Adv. Funct. Mater., 26 (2016) 8334-8344.

[19] Q. Lai, L. Zheng, Y. Liang, J. He, J. Zhao, J. Chen, Metal-organic-framework-derived Fe-N/C electrocatalyst with five-coordinated Fe-Nx sites for advanced oxygen reduction in acid media, ACS Catal., 7 (2017) 1655-1663.
[20] A. Mahmood, W. Guo, H. Tabassum, R. Zou, Metal-organic framework-based nanomaterials for electrocatalysis, Adv. Energy Mater., 6 (2016) 1600423.
[21] Q.L. Zhu, W. Xia, T. Akita, R. Zou, Q. Xu, Metal-organic framework-derived honeycomb-like open porous nanostructures as precious-metal-free catalysts for highly efficient oxygen electroreduction, Adv. Mater., 28 (2016) 6391-6398.
[22] L. Zhang, Z. Su, F. Jiang, L. Yang, J. Qian, Y. Zhou, W. Li, M. Hong, Highly graphitized nitrogen-doped porous carbon nanopolyhedra derived from ZIF-8 nanocrystals as efficient electrocatalysts for oxygen reduction reactions, Nanoscale, 6 (2014) 6590-6602.
[23] Q. Lin, X. Bu, A. Kong, C. Mao, F. Bu, P. Feng, Heterometal-embedded organic conjugate frameworks from alternating monomeric iron and cobalt metalloporphyrins and their application in design of porous carbon catalysts, Adv. Mater., 27 (2015) 3431-3436.
[24] A. Kong, Q. Lin, C. Mao, X. Bu, P. Feng, Efficient oxygen reduction by nanocomposites of heterometallic carbide and nitrogen-enriched carbon derived from the cobalt-encapsulated indium-MOF, Chem. Commun., 50 (2014) 15619-15622.
[25] J. Pampel, T.P. Fellinger, Opening of bottleneck pores for the improvement of nitrogen doped carbon electrocatalysts, Adv. Energy Mater., 6 (2016) 1502389.
[26] Y. He, D. Gehrig, F. Zhang, C. Lu, C. Zhang, M. Cai, Y. Wang, F. Laquai, X. Zhuang, X. Feng, Highly efficient electrocatalysts for oxygen reduction reaction based on

1D ternary doped porous carbons derived from carbon nanotube directed conjugated microporous polymers, Adv. Funct. Mater., 26 (2016) 8255-8265.

[27] W. Gu, L. Hu, J. Li, E. Wang, Iron and nitrogen co-doped hierarchical porous graphitic carbon for a high-efficiency oxygen reduction reaction in a wide range of pH, J. Mater. Chem. A, 4 (2016) 14364-14370.

[28] K. Gong, F. Du, Z. Xia, M. Durstock, L. Dai, Nitrogen-doped carbon nanotube arrays with high electrocatalytic activity for oxygen reduction, Science, 323 (2009) 760.

[29] L. Li, J. He, Y. Wang, X. Lv, X. Gu, P. Dai, D. Liu, X. Zhao, Metal–organic frameworks: a promising platform for constructing non-noble electrocatalysts for the oxygen-reduction reaction, J. Mater. Chem. A, 7 (2019) 1964-1988.

[30] L. Li, P. Dai, X. Gu, Y. Wang, L. Yan, X. Zhao, High oxygen reduction activity on a metal–organic framework derived carbon combined with high degree of graphitization and pyridinic-N dopants, J. Mater. Chem. A, 5 (2017) 789-795.

[31] Q.-L. Zhu, Q. Xu, Metal-organic framework composites, Chem. Soc. Rev., 43 (2014) 5468-5512.

[32] Y. Wang, X. Chen, Q. Lin, A. Kong, Q.-G. Zhai, S. Xie, P. Feng, Nanoporous carbon derived from a functionalized metal-organic framework as a highly efficient oxygen reduction electrocatalyst, Nanoscale, 9 (2017) 862-868.

[33] R. Wang, X.Y. Dong, J. Du, J.Y. Zhao, S.Q. Zang, MOF-derived bifunctional Cu_3P nanoparticles coated by a N,P-codoped carbon shell for hydrogen evolution and oxygen reduction, Adv. Mater., 30 (2018) 1703711.

[34] J. Zhou, Y. Dou, A. Zhou, R.M. Guo, M.J. Zhao, J.R. Li, MOF template-directed fabrication of hierarchically structured electrocatalysts for efficient oxygen evolution Reaction, Adv. Energy Mater., 7 (2017) 1602643.

[35] G. Cai, W. Zhang, L. Jiao, S.-H. Yu, H.-L. Jiang, Template-directed growth of well-aligned MOF arrays and derived self-supporting electrodes for water splitting, Chem, 2 (2017) 747-748.

[36] C. Mao, A. Kong, Y. Wang, X. Bu, P. Feng, MIL-100 derived nitrogen-embodied carbon shells embedded with iron nanoparticles, Nanoscale, 7 (2015) 10817-10822.

[37] Z. Jiang, H. Sun, Z. Qin, X. Jiao, D. Chen, Synthesis of novel ZnS nanocages utilizing ZIF-8 polyhedral template, Chem. Commun., 48 (2012) 3620-3622.

[38] A.D. Roberts, J.-S.M. Lee, S.Y. Wong, X. Li, H. Zhang, Nitrogen-rich activated carbon monoliths via ice-templating with high CO_2 and H_2 adsorption capacities, J. Mater. Chem. A, 5 (2017) 2811-2820.

[39] J. Kou, L.-B. Sun, Fabrication of nitrogen-doped porous carbons for highly efficient CO_2 capture: rational choice of a polymer precursor, J. Mater. Chem. A, 4 (2016) 17299-17307.

[40] F. Sun, X. Liu, J. Gao, X. Pi, L. Wang, Z. Qu, Y. Qin, Highlighting the role of nitrogen doping in enhancing CO_2 uptake onto carbon surfaces: a combined experimental and computational analysis, J. Mater. Chem. A, 4 (2016) 18248-18252.

[41] H.x. Zhong, J. Wang, Y.w. Zhang, W.l. Xu, W. Xing, D. Xu, Y.f. Zhang, X.b. Zhang, ZIF-8 Derived graphene-based nitrogen-doped porous carbon sheets as highly efficient and durable oxygen reduction electrocatalysts, Angew. Chem. Int. Ed., 53 (2014) 14235-14239.

[42] K. Elumeeva, J. Ren, M. Antonietti, T.P. Fellinger, High surface iron/cobalt-containing nitrogen-doped carbon aerogels as non-precious advanced electrocatalysts for oxygen reduction, ChemElectroChem, 2 (2015) 584-591.

[43] M. Graglia, J. Pampel, T. Hantke, T.-P. Fellinger, D. Esposito, Nitro Lignin-derived nitrogen-doped carbon as an efficient and sustainable electrocatalyst for oxygen reduction, ACS nano, 10 (2016) 4364-4371.

[44] A. Aijaz, N. Fujiwara, Q. Xu, From metal-organic framework to nitrogen-decorated nanoporous carbons: high CO_2 uptake and efficient catalytic oxygen reduction, J. Am. Chem. Soc., 136 (2014) 6790-6793.

[45] J. Zhou, Z. Li, W. Xing, H. Shen, X. Bi, T. Zhu, Z. Qiu, S. Zhuo, A new approach to tuning carbon ultramicropore size at sub-angstrom level for maximizing specific capacitance and CO_2 uptake, Adv. Funct. Mater., 26 (2016) 7955-7964.

[46] L. Liu, Z.-H. Xie, Q.-F. Deng, X.-X. Hou, Z.-Y. Yuan, One-pot carbonization enrichment of nitrogen in microporous carbon spheres for efficient CO_2 capture, J. Mater. Chem. A, 5 (2017) 418-425.

[47] A. Aijaz, T. Akita, H. Yang, Q. Xu, From ionic-liquid@metal-organic framework composites to heteroatom-decorated large-surface area carbons: superior CO_2 and H_2 uptake, Chem. Commun., 50 (2014) 6498-6501.

[48] Y. Kojima, Y. Kawai, A. Koiwai, N. Suzuki, T. Haga, T. Hioki, K. Tange, Hydrogen adsorption and desorption by carbon materials, J. Alloys Compd., 421 (2006) 204-208.

[49] M. Sevilla, R. Mokaya, Energy storage applications of activated carbons: supercapacitors and hydrogen storage, Energy Environ. Sci., 7 (2014) 1250-1280.